

Journal of Thermoplastic Composite Materials

<http://jtc.sagepub.com>

Strain Monitoring in Thermoplastic Composites with Optical Fiber Sensors: Embedding Process, Visualization with Micro-tomography, and Fatigue Results

I. De Baere, E. Voet, W. Van Paepegem, J. Vlekken, V. Cnudde, B. Masschaele and J. Degrieck

Journal of Thermoplastic Composite Materials 2007; 20; 453

DOI: 10.1177/0892705707082325

The online version of this article can be found at:
<http://jtc.sagepub.com/cgi/content/abstract/20/5/453>

Published by:

 SAGE Publications

<http://www.sagepublications.com>

Additional services and information for *Journal of Thermoplastic Composite Materials* can be found at:

Email Alerts: <http://jtc.sagepub.com/cgi/alerts>

Subscriptions: <http://jtc.sagepub.com/subscriptions>

Reprints: <http://www.sagepub.com/journalsReprints.nav>

Permissions: <http://www.sagepub.com/journalsPermissions.nav>

Strain Monitoring in Thermoplastic Composites with Optical Fiber Sensors: Embedding Process, Visualization with Micro-tomography, and Fatigue Results

I. DE BAERE,^{1,*} E. VOET,² W. VAN PAEPEGEM,¹
J. VLEKKEN,² V. CNUDDÉ,³ B. MASSCHAELE⁴ AND J. DEGRIECK¹

¹*Faculty of Engineering, Department of Mechanical Construction and Production, Ghent University, Sint-Pietersnieuwstraat 41 B-9000 Gent, Belgium*

²*FOS&S, Fibre Optic Sensors & Sensing Systems Ciplastraat 14, B-2440 Geel, Belgium*

³*Faculty of Science, Department of Geology and Soil Science Ghent University, Krijgslaan 281 S8, B-9000 Gent, Belgium*

⁴*Faculty of Science, Department of Subatomic and Radiation Physics Ghent University, Proeftuinstraat 86, B-9000 Gent, Belgium*

ABSTRACT: This study investigates the possibility of using optical fibers with Bragg gratings for measurements under fatigue loading conditions. Detailed information is given on the principle of optical fiber measurements, the embedding process, and the fatigue tests. To verify the strain derived from the optical fiber, the strain is compared with extensometer measurements. A special design of the blades of the extensometer is presented, since the standard blades suffer from a loss of grip on the surface of the specimen. Furthermore, X-ray micro-tomography is discussed and used for the visualization of the optical fibers and damage in the composite material. The material used for this study is a carbon fiber-reinforced polyphenylene sulfide. It can be concluded that the optical fiber survives over half a million loading cycles, without de-bonding of the fiber. Furthermore, the resolution of the micro-tomography is high enough to visualize not only the optical fiber, but also damage in the material.

KEY WORDS: fiber Bragg grating, thermoplastic composite fatigue, micro-tomography.

*Author to whom correspondence should be addressed. E-mail: Ives.DeBaere@UGent.be

INTRODUCTION

THE CLASSICAL METHODS for periodical maintenance of composite structures, for example airplanes, use many NDE techniques (e.g., ultrasound, radiography, and thermography). However, these techniques require extensive human involvement and expensive procedures. Moreover, this kind of periodical inspection cannot give any information concerning accidents or failures occurring between two successive overhauls. In order to overcome such shortcomings it is now possible to use 'sensitive' materials, which means the material includes sensors providing real-time information about the material itself, e.g., embedded optical fibers. These sensors are embedded together with the other reinforcement fibers and are capable of carrying loads. An average optical fiber is about 125μ in diameter, which is about ten times as much as the average carbon fiber (10μ). Because of the load carrying capability however, they have limited influence on the mechanical behavior. The feasibility of optical fiber sensors for monitoring the mechanical behavior is already studied in [1,2] for a thermosetting matrix, with good result.

It was even concluded that optical fiber Bragg sensors were more reliable than classical strain gages [1]. Doyle et al. [3] experimented on the use of fiber optic sensors for tracking the cure reaction of a fiber-reinforced epoxy, with success. They also successfully demonstrated the feasibility of these sensors for monitoring the stiffness reduction due to fatigue damage, but for thermosetting matrix. The latter was also done by Shin and Chiang [4,5] for a carbon fiber-reinforced epoxy.

In this study, the use of fiber Bragg gratings (FBGs) for fatigue experiments is investigated for a carbon fiber-reinforced thermoplastic, namely a polyphenylene sulfide (PPS). The latter is known for its chemical inertness, which means that de-bonding of the fiber may be a problem. Therefore, extra attention is given to the embedding of the fiber. In order to visualize the embedded fiber, X-ray micro-tomography is used. The feasibility of the latter is also assessed for visualizing fatigue damage.

In the following paragraph, the used materials are discussed. Next, the principles of optical fiber measurement and X-ray micro-tomography are explained. This is followed by some details about the embedding of the fiber and the visualizing of this sensor using micro-tomography. Next, the results of the fatigue tests are discussed. The special design of the extensometer blades, used for these tests, is illustrated. Then, some results of the micro-tomography, concerning the capability of assessing damage, are presented. Finally, some conclusions are drawn.

MATERIALS AND METHODS

Composite Material

The material used for the fatigue experiments was a carbon fiber-reinforced PPS, called CETEX[®]. This material was supplied by Ten Cate Advanced Composites (The Netherlands). The fiber type is the carbon fiber T300 J 3 K and the weaving pattern is a five-harness satin weave with a mass per surface unit of 286 g/m². The five-harness satin weave is a fabric with high strength in both directions and excellent bending properties.

The carbon PPS plates were hot pressed, two stacking sequences were used for this study, namely [(0°,90°)]_{2s} and [(0°,90°)]_{4s} where (0°,90°) represents one layer of fabric.

The in-plane elastic properties of the individual carbon PPS lamina were determined by the dynamic modulus identification method as described in [6] and are listed in Table 1.

The tensile strength properties were determined at the Technical University of Delft and are listed in Table 2. Because of the used composite lay-ups previously mentioned, the mechanical properties given for the lamina also apply for the laminate. The test coupons were cut with a water-cooled diamond saw. The dimensions of the coupons used for fatigue experiments were chosen according to the ASTM D3479 tension–tension fatigue and are shown in Figure 1. It was attempted to have the grating of the fiber somewhere in the middle.

Table 1. In-plane elastic properties of the individual carbon-PPS lamina (dynamic modulus identification method).

E_{11}	56.0	GPa
E_{22}	57.0	GPa
ν_{12}	0.033	–
G_{12}	4.175	GPa

Table 2. Tensile strength properties of the individual carbon-PPS lamina (mechanical testing at TUDelft).

X_T	617.0	MPa
$\varepsilon_{11}^{\text{ult}}$	0.011	–
Y_T	754.0	MPa
$\varepsilon_{22}^{\text{ult}}$	0.013	–
S_T	110.0	MPa

Optical Fibers

The principle of an optical fiber sensor with a Bragg grating is illustrated in Figure 2.

Broadband light is transmitted into the optical fiber. At a specific point in this fiber, there is a Bragg grating, which acts as a wavelength selective mirror. For each grating only one wavelength, the Bragg wavelength, λ_B is reflected with a full width at half maximum of typically 100 pm, while all other wavelengths are transmitted. As a result, an optical fiber can be read out from both ends of the fiber.

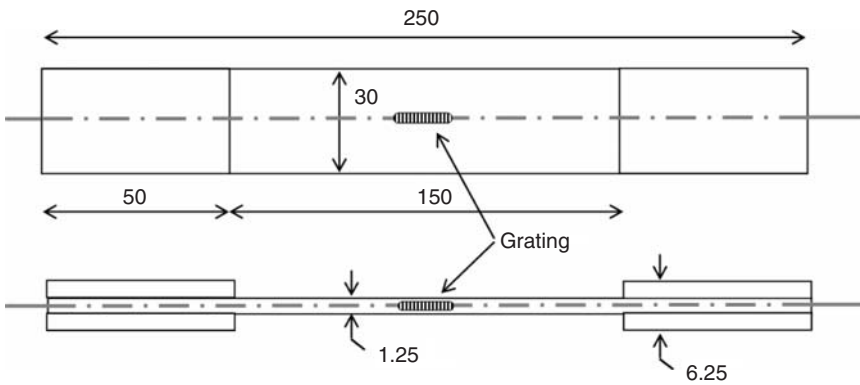


Figure 1. Dimensions of the used tensile coupon, equipped with tabs.

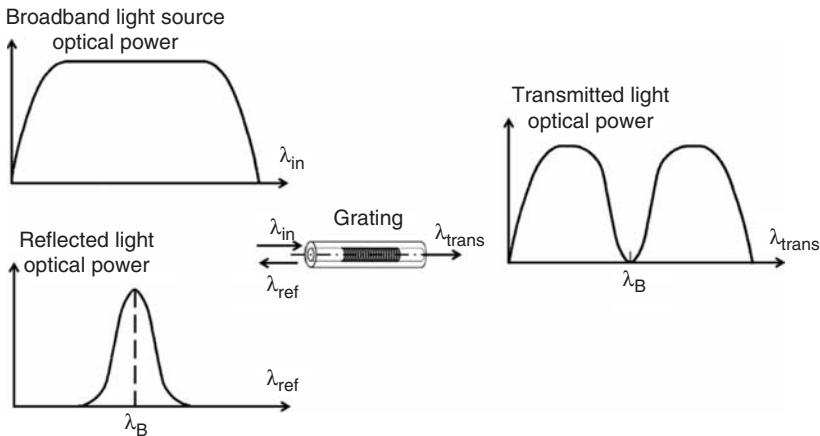


Figure 2. The principle of an optical fiber Bragg grating (FBG).

A FBG is actually no more than an area in the core of the fiber with successive zones with an alternating refractive index. If Λ is the period of the grating, then the Bragg wavelength of the grating is given by:

$$\lambda_B = 2n_{\text{eff}}\Lambda \quad (1)$$

where n_{eff} is an averaged refractive index over the length L of the grating.

To better understand the strain sensing principle of an FBG, one has to first derive the basic Bragg condition (1). Taking the differential yields:

$$d\lambda = 2 \left[\frac{\partial n_{\text{eff}}}{\partial \varepsilon} \Lambda + n_{\text{eff}} \frac{\partial \Lambda}{\partial \varepsilon} \right] d\varepsilon + 2 \left[\frac{\partial n_{\text{eff}}}{\partial T} \Lambda + n_{\text{eff}} \frac{\partial \Lambda}{\partial T} \right] dT. \quad (2)$$

By using the Bragg condition of (1) on all four terms in (2), this equation can be rewritten as:

$$d\lambda = \lambda_B \left[\frac{1}{n_{\text{eff}}} \frac{\partial n_{\text{eff}}}{\partial \varepsilon} + \frac{1}{\Lambda} \frac{\partial \Lambda}{\partial \varepsilon} \right] d\varepsilon + \lambda_B \left[\frac{1}{n_{\text{eff}}} \frac{\partial n_{\text{eff}}}{\partial T} + \frac{1}{\Lambda} \frac{\partial \Lambda}{\partial T} \right] dT. \quad (3)$$

Since $\partial \Lambda / \Lambda = \partial \varepsilon$ and assuming the strain and temperature variations are small, the differentials in Equation (3) can be replaced by differences.

By defining:

$$\begin{cases} P = -\frac{1}{n_{\text{eff}}} \frac{\partial n_{\text{eff}}}{\partial \varepsilon} = \frac{n_{\text{eff}}^2}{2} (p_{12} - \nu(p_{11} + p_{12})) \\ \alpha_n = \frac{1}{n_{\text{eff}}} \frac{\partial n_{\text{eff}}}{\partial T} \\ \alpha_f = \frac{1}{\Lambda} \frac{\partial \Lambda}{\partial T} \end{cases} \quad (4)$$

with P the effective photo-elastic coefficient or strain-optic coefficient, p_{11} and p_{12} the elasto-optic coefficients of the strain-optic tensor, ν the Poisson's ratio, α_n the thermo-optic constant, and α_f the thermal expansion coefficient of the fiber. Substituting these coefficients in Equation (3) yields:

$$\frac{\Delta \lambda}{\lambda_B} = (1 - P)\Delta \varepsilon + (\alpha_n + \alpha_f)\Delta T. \quad (5)$$

Some material constants used to calculate the strain-sensitivity of GeO₂ doped silica glass-fiber are:

- Effective refractive index $n_{\text{eff}} = 1.45$
- Poisson's ratio: $\nu = 0.16$

- Elasto-optic constants: $p_{11} = 0.113$
- the thermo-optic constant $p_{12} = 0.252$
- the thermal expansion coefficient $\alpha_n = 5.9 \cdot 10^{-6} \text{ K}^{-1}$
- the thermal expansion coefficient $\alpha_f = 0.55 \cdot 10^{-6} \text{ K}^{-1}$

The value for α_n is a weighted mean value confirmed by a number of experiments and temperature calibrations. Together with the FBG-wavelength, these coefficients determine the linear strain and temperature sensitivities:

$$\begin{aligned} s_S &= (1 - P) \cdot \lambda_B = 0.796 \cdot \lambda_B \\ s_T &= (\alpha_n + \alpha_f) \cdot \lambda_B = 6.45 \cdot 10^{-6} \cdot \lambda_B. \end{aligned} \quad (6)$$

With this, the linear approximation becomes:

$$\Delta\lambda = s_S \Delta\varepsilon + s_T \Delta T. \quad (7)$$

Typical values for S_S and S_T for an FBG in the C-band region (1520–1560 nm) are 1.2 pm/ $\mu\varepsilon$ and 10 pm/ $^\circ\text{C}$, respectively. It should be noted that these sensitivities are in fact wavelength dependent – they are directly proportional to the FBG-wavelength λ_B – but for small wavelength changes they are normally approximated as being constant.

Since an FBG is sensitive for both strain and temperature, two FBGs are needed, one to measure strain and one to measure temperature. The latter is necessary to compensate for wavelength shifts due to temperature fluctuations. A relatively easy method to achieve this is to use a capillary or a ferrule design where the second FBG is kept strain-free. This is illustrated in Figure 3. Grating 1 is affected by both the strain and the temperature of the surrounding composite, whereas Grating 2 only sees the temperature, because the fiber ends in the capillary and therefore is not strained. By subtracting the shift in wavelength in Grating 2 from the shift in Grating 1, the strain measurement is realized and the shift in Grating 2 represents the temperature.

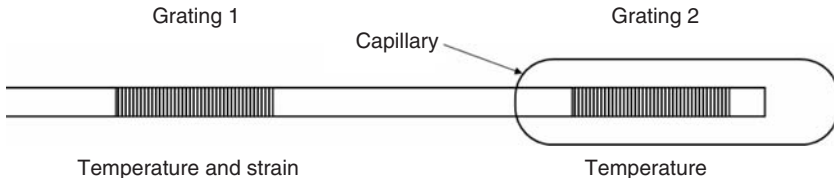


Figure 3. Illustration of the use of a capillary for the compensation of temperature effects.

Previous fatigue experiments on the composite under study revealed no significant temperature increase during the experiment, so no capillary was embedded.

If the temperature during the experiment is constant, then the second term in Equation (7) can be omitted and a measurement of the strain is achieved: the difference between the wavelength of the strained and the unstrained grating increases linearly with the imposed strain (Equation (7)) and the sensitivity is $1.2 \text{ pm}/\mu\epsilon$ at the operating wavelength of $1.5 \mu\text{m}$.

This is an absolute value, since it only depends on the geometry of the grating and the elasto-optic constants of the glass, and not on any form of electronic manipulation, such as filtering or amplifying. Furthermore, it has to be noticed that a FBG written in hydrogenated fibers will notice a decrease in refractive index modulation of $\approx 15\%$ [7] hence a drift of Bragg wavelength and decrease of reflection of about 9% in the first few weeks after fabrication of the grating. However this is not the case for gratings written in non-hydrogenated fibers [8], as is the case for the FBG employed in these experiments. As such, the Bragg wavelength of these sensors does not drift away in time as can be the case with strains, derived from strain gage measurements. The used data acquisition system has an accuracy of 5 pm and it is constant in time. Therefore, this system also does not cause a drift of the measurement.

The choice of the characteristic wavelength λ_B depends on the type of experiment and the data acquisition unit. The latter will be able to register only a certain range of wavelengths and has a certain bandwidth in the C-band region (1520–1560 nm) that is determined by the optical source of the interrogator. If the experiment is pure tension, λ_B should be chosen near the lower boundary of that range and if the experiment is pure compression, λ_B should be chosen near the upper boundary of that range. The outer boundary should not be chosen, since hot pressing introduces unknown stresses and as a result, a small shift in λ_B [1,9].

The fiber optic sensors used for these embedding experiments are uniform draw tower FBGs (DTG[®]s), provided by FBGS-Technologies GmbH, Jena (Germany). Such gratings are manufactured during the fabrication process of the optical fiber and are coated just after the inscription of the Bragg grating [10]. These draw tower FBGs (manufactured by FBGS-technologies) have a uniform index profile (i.e., not chirped or tapered) and are fabricated during the drawing of the fiber. They have a reflectivity typically 15–20% with nominal wavelengths typically in the range of 1520–1575 nm. The method employed for inscribing gratings over such a wide wavelength range is a complex method or technology based on a Talbot interferometer which makes it possible to change the design wavelength simply by changing the angle of the two mirrors which unite the diffracted laser beams at the center

of the fiber [10]. Owing to the combination of these two first-order laser bundles, an interference pattern with a defined length is induced and thus a FBG with a specific Bragg wavelength is created at that exact spot.

The FBGs are written in a (special) single mode optical fiber with core- and cladding-diameter of 6 and 125 μm , respectively. Such a special single mode fiber is made of fused silica (SiO_2) with a highly Ge-doped (GeO_2) core ($\approx 18\text{ mol}\%$) for high photosensitivity, necessary for inducing the periodic refractive index pattern with a single laser shot during the draw tower process and thus creating the Bragg grating sensor.

Fiber draw tower gratings have a core diameter of 6 μm , a cladding diameter of 125 μm , and an outer diameter, with ORMOCER coating (ORGANIC MODIFIED CERAMIC), of 195 μm . This diameter is about the same as a carbon fiber bundle or fabric ($\approx 320\ \mu\text{m}$).

The ORMOCER coating material provides excellent mechanical properties such as an ultimate strain value between 5 and 6%. It should be noted that the ORMOCER has good bonding properties with the glass surface of the optical fiber and therefore this optical fiber has very good sensor properties for strain measurements. Also a good adhesion with the PPS matrix is found, even after half a million cycles the FBG sensors showed no signs of de-bonding (see section on fatigue experiment).

An important remark about the optical data acquisition unit must be made. The swept laser interrogator (SLI) has a sampling frequency of 100 Hz. However, it does not use a sample and hold principle, but it reads continuously. The difference between the two is illustrated in Figure 4 where the illustrated sinusoidal signal has a frequency of 5 Hz.

The 'sample and hold' principle freezes the registered value until the data acquisition unit has finished processing it. For the continuous measurement,

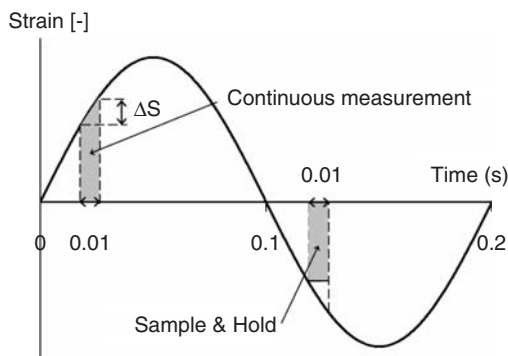


Figure 4. Illustration of the difference between a sample and hold and a continuous measurement.

the registration takes $1/f$ s, f being the sample frequency, to gather the data. Since the SLI samples at 100 Hz, it takes 0.01 s for the measurement. Since the loading frequency during the fatigue tests is 5 Hz, this sampling rate is too slow. There is already a large difference in the occurring strain at time t and $t + 0.01$ s. To overcome this problem, the fatigue experiment was paused after a certain number of cycles and a quasi-static tensile test was performed with a pulling speed of 2 mm/min (see section on fatigue experiment).

With a sampling rate of 100 Hz, the difference in the occurring strain at time t and at $t + 0.01$ s is small enough and will be maximum $2.22 \mu\epsilon$. As such, the error made when performing the intermediate quasi-static testing is very small, on the order of a few micro-strains, and can be neglected in further calculations.

However when higher sampling frequencies are required one should look for a solution to synchronize data in a more sophisticated way. Improved software or another device which operates with the sample and hold principle, could definitely offer the possibility to measure dynamically during fatigue loading.

Micro-tomography

High-resolution 3D X-ray micro-tomography or micro-CT is a relatively new technique which allows scientists to investigate the internal structure of their samples without actually opening or cutting them. Without any form of sample preparation, 3D computer models of the sample and its internal features can be produced with this technique. The physical parameter, providing the information about the structure, is the X-ray attenuation coefficient μ . This coefficient is the product of the photon mass attenuation coefficient μ/ρ (cm^2/g) and the chemical density ρ (g/cm^3). The attenuation coefficient μ depends on the local composition of the material of the sample.

Furthermore, the mass attenuation coefficient depends on the energy of the X-rays: the higher the energy of the photon, the smaller the attenuation in the sample. Portable X-ray sources are producing the X-rays, while X-ray detectors are used to record the attenuation information along lines through the object and register the image as a radiograph. In order to perform tomography, digital radiographs of the sample are made from different orientations by rotating the sample along the scan axis from 0 to 360° . After collecting all the projection data, the reconstruction process produces 2D horizontal cross-sections of the scanned sample. These 2D images can then be rendered into 3D models, which enable to virtually look into the object. Special 3D software, Morpho+ [11] is developed in order to obtain 3D data of the internal features, including volume distributions, porosity, pore sizes, etc.

For this study, the high power directional tube with a conical tungsten anode and an aluminum exit window, which attenuates most of the X-rays below 10 keV, of the dual head 160 kV Feinfocus[®] open-type tube X-ray source was used. With a maximum power of 150 W and a high X-ray power output, the directional tube is perfectly suited to penetrate the thermoplastic composites. The X-ray detector, a remote Radeye EV CMOS flat panel (<http://www.rad-icon.com>) was applied. This detector provides a high contrast for micro-focus CT, with X-ray tube voltages up to 160 kV. Its active area is 24.6 mm by 49.2 mm and consists of a 512 by 1024 matrix of silicon photodiodes on 48 μm centers. A thin straight fiber optic coupling is used to transport the visible light from the phosphor to the CMOS. The samples are positioned on a highly sensitive sample manipulator, consisting of seven motor stages. The samples are positioned between the X-ray tube and the X-ray detector with an XYZ-translation stage with Berger Lahr stepper motors (IcIA IFS). To reach the high precision CT-scan, a rotation stage with air bearing (MICOS, UPR160F-AIR) is used. A standard air compressor and a series of filters provide 4.5 bar air pressure for the stage. Additionally, an XY-piezo stage with 50 nm resolution and 20 mm travel range is fixed on the rotation platform to center the sample on the rotation axis.

Tensile Testing Machine

All tensile tests were performed on a servo-hydraulic INSTRON 1342 tensile testing machine with a FastTrack 8800 digital controller and a load cell of ± 100 kN.

For the strain measurements, strain gages could not be used, since they tend to de-bond after a few thousands of cycles. Furthermore, PPS is not easily bonded with adhesives. Therefore, an extensometer was mounted on the specimen. The blades of the extensometer however, tended to loose grip on the very smooth surface of the thermoplastic composite. A different design of the blades was used. This design is discussed later.

For the registration of the tensile data, a combination of a National Instruments DAQpad 6052E for FireWire, IEEE 1394, and the SCB-68 pin shielded connector were used. The load, displacement, and strain, given by the FastTrack controller, as well as the extra signal from the thermocouple were sampled on the same time basis.

For the registration of the optical data, an SLI 1000 system was used. This system uses a tuneable laser as light source which is swept across a broad spectrum at 100 Hz with a bandwidth of ≈ 38 nm in the C-Band range (1520–1558 nm). The reflected wavelength was measured during quasi-static

loading at a frequency of 100 Hz and afterwards, this signal was sampled at the same time basis as the signal obtained from the tensile machine, to be able to compare them. Experimental results are presented in the section on fatigue experiment where it is demonstrated that the strain measured with the extensometer correlates with the strain monitored with the embedded FBG.

EXPERIMENTS AND DISCUSSION

The Embedding of the Fiber

Carbon fiber-reinforced PPS plates, CETEX[®], with $[(0^\circ, 90^\circ)]_{2s}$ stacking sequence are fabricated by piling a number of semi-preg layers (with reinforcement fibers woven in 0° and 90°) and by pressing them together with appropriate pressure and temperature. Optical fibers can be put in between two layers of semi-preg (completely impregnated with PPS polymer) and can be fixated in orientation at will simply by using an ultrasonic welding device and a small piece of PPS-sheet to fix the fiber at the semi-preg layer.

If a composite material with embedded optical fiber is considered, it is important that there is minimum or zero disturbance on the matrix and structural behavior of the composite. Thin plates compiled of only four laminae were used to investigate if the optical fiber showed any significant influence on the material properties. The fibers were put between Laminae 2 and 3 and the composite plate is manufactured by pressing the layers together in a hot mold at a pressure of 10 bar and a temperature of $\approx 320^\circ\text{C}$ for a few hours and further cooled-off with air- and water-cooling till room temperature.

Considering the dimensions of such semi-preg layers (thickness $\approx 320\ \mu\text{m}$) one would say optical fibers with a coating diameter of $195\ \mu\text{m}$ could induce local disturbance in the matrix and influence the structural behavior of the composite. However, fatigue tension tests showed positive results indicating that the fiber optic sensor has little or no effect on the mechanical properties of the composite plate.

In addition, the coating of the optical fiber should have a good adhesion with the matrix-material, so strain inside the composite is transmitted well. Fatigue testing relieved with quasi-static testing showed a good transmission of strain to the DTG[®] with ORMOCER coating and showed no significant difference in mechanical properties in comparison with samples without embedded optical fiber (see the section on fatigue experiment). The ORMOCER coating has proven to be a well suited coating for embedding in CETEX[®] material.

Further investigations on reducing the fiber diameter and/or coating material and diameter will be done in order to optimize the draw tower FBG for embedding in the CETEX[®] material.

Visualizing the Fiber

Because of the high resolution achieved with the glass fiber-reinforced epoxy, the micro-tomography should be able to visualize the optical fiber. Since the thickness of the four-layer stacking sequence is only 1.25 mm, it is hard to machine a beam like test sample for the micro-tomography. Therefore, a few samples were machined and then taped together. The orientation of the top and bottom specimens differed 90° with the central one, to have a clear view of the fibers, both longitudinal and transverse. The taped specimens are shown in Figure 5. The optical fiber is clearly visible between the second and third layers.

The CT data were reconstructed with Octopus (<http://www.xraylab.com>) and for the 3D rendering, the software VGStudiomax (www.volumegraphics.com) was used. The 3D-volume can be cut in different sections. The position of the cut was chosen so that all three fibers were visible. This is shown in Figure 6. All three fibers are clearly visible. Again, the accuracy of this method is illustrated; the coating of the optical fiber is noticeable.

Fatigue Experiment

To assess whether the optical fiber is capable of measuring strains during the entire lifetime of the composite specimen, several fatigue tests

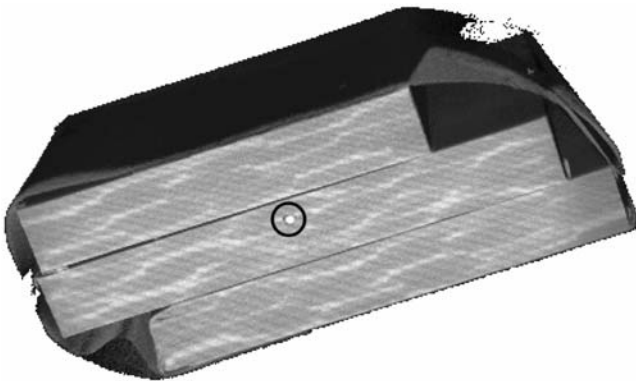


Figure 5. Three-dimensional image of the three samples (taped together) of $[(0^\circ, 90^\circ)]_{2s}$ carbon-PPS with optical fiber.

were performed. As was mentioned in the previous paragraph, it is not possible to read the optical fiber during the fatigue test, so seven quasi-static tensile tests were performed. The first static test was done before the fatigue experiment was started and the test was stopped after the seventh static test. The fatigue test was not done till fracture, so that this specimen could still be examined with micro-tomography. The optical fiber in the specimen had a starting wavelength of 1556 nm. The latter is relatively high for a tensile test, but this wavelength was chosen for the monitoring of the production process of the plate. The quasi-static tests were displacement-controlled with a speed of 2 mm/min, the fatigue tests were force controlled with σ_{\max} equal to 300 MPa, which is about 50% of the ultimate stress (Table 2), and σ_{\min} equal to 0 MPa and a loading frequency of 5 Hz. The latter is a compromise between (i) heat generation, which occurs at higher frequencies and (ii) duration of the test.

To verify if the optical fiber strain is accurate, an accurate longitudinal strain measurement for comparison is required. The latter is achieved by mounting an extensometer on the specimen. However, in previous fatigue tests, it was noticed that the blades of the extensometer lost their grip on the smooth surface of the PPS, causing a sudden jump in the strain. Since the test was done in load control, this did not cause any problems. However, for a strain controlled test, this would ruin the entire experiment and possibly damage the tensile testing machine. Furthermore, the strain measurement would not be accurate enough for comparison with the optical fiber. Therefore, a modified design of the blades was tested. The normal blades of the extensometer, as well as the new design are shown in Figure 7.

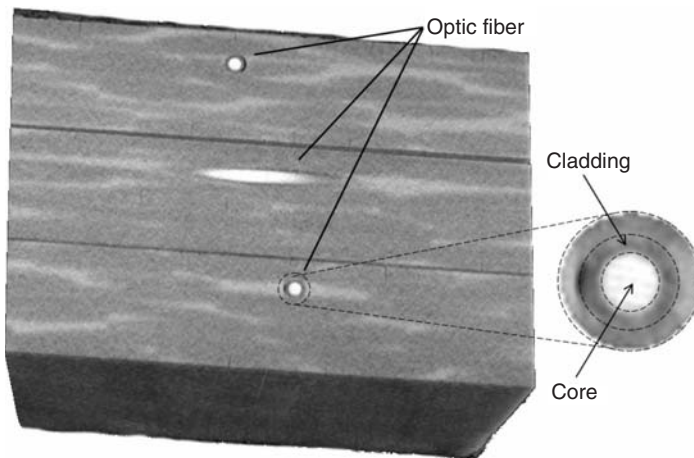


Figure 6. Cut of the 3D-image of the taped $[(0^\circ, 90^\circ)]_{2s}$ carbon-PPS samples.

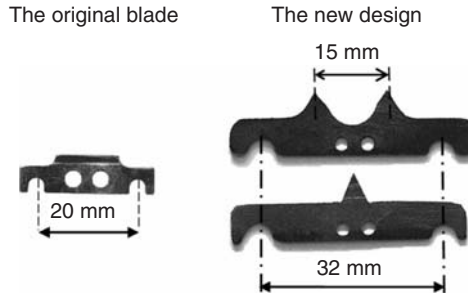


Figure 7. Illustration of the extensometer blades.

The new design improves two critical points of the original blades:

- (i) The original blades make a line contact. It is very difficult to have two blades that are exactly parallel, so that in most of the cases, the two edges cross and therefore make a bad contact. In the new design, one blade makes contact with one point, while the other blade makes contact with two points. Since three points define a surface, these points always make a good contact with the specimen.
- (ii) The width of the original blades was too small in comparison with the width of the specimen. With the new wider blades, higher contact forces are achieved, which should prevent sudden jumps in the strain measurement.

The new design was then calibrated in order to have accurate measurements.

Figure 8 illustrates the measured strains, both with the extensometer and the optical fiber. The strain is plotted as a function of the time (s), the different curves are given a certain offset with respect to each other, to have a clear image. Underneath each measurement, the corresponding cycle is noted; the first curve corresponds with the initial static test.

The results correspond perfectly. The small plateau at the end of the optical measurement is due to the saturation of the optical data acquisition unit, it corresponds with a wavelength of 1560 nm. The extensometer measurement was stopped a little after the SLI saturated.

It may be noticed that the strain for the first static test increases slower than for all the other tests. This is due to slipping of the clamps.

To verify whether the temperature had any effect on the measurements, the temperature on the surface of the specimen was monitored using a type K thermocouple. The results of this measurement are shown in Figure 9. It may be noticed that no heat is generated at the surface of the specimen during this fatigue test. As a result, the influence of the temperature on the optical fiber measurement may be neglected, since the

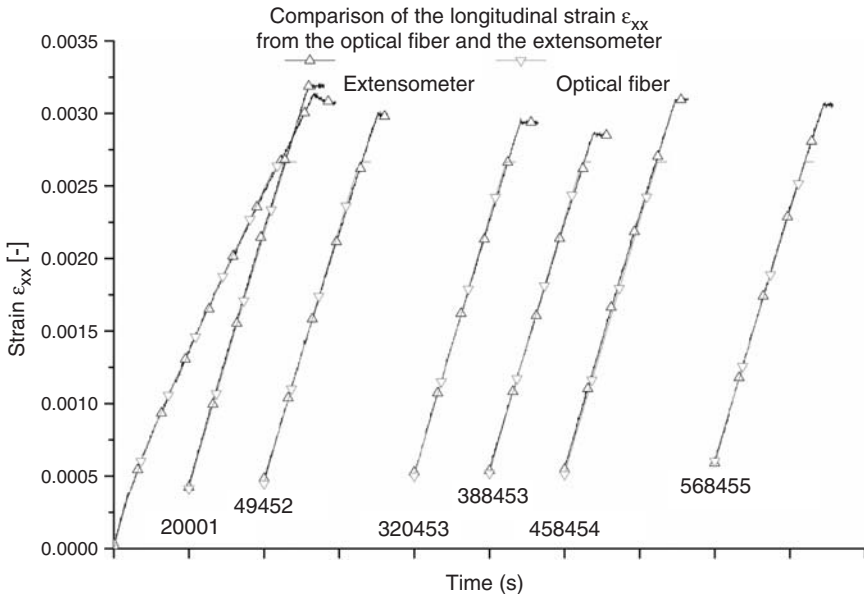


Figure 8. Comparison of the different longitudinal strains, as a function of the time.

effect of the strain on the Bragg wavelength (first term in Equation (7)) is dominant over the temperature effect on the wavelength (second term in Equation (7)). Taking the noise into account, the maximum temperature difference is about 1°C , corresponding to 10 pm shift in wavelength; the increase in strain is about $3000\text{ }\mu\epsilon$, corresponding to 3600 pm shift in wavelength.

The stress-strain curves, corresponding to these static tests, are shown in Figure 10, together with the corresponding stiffness. It must be noted that there is no stiffness degradation and only very limited permanent deformation, even after more than half a million cycles. In [5] a significant stiffness reduction was found, but for a carbon fiber-reinforced epoxy. This illustrates the differences of fatigue behavior of thermosetting and thermoplastic matrices.

It may be noticed that the stiffness increases after the second, the fourth, and the sixth tensile tests. This is due to scatter on the measurement and it is visible because there is no stiffness degradation.

To verify whether the optical fiber has an influence on the stiffness of the laminate and to test the new extensometer blades, another fatigue experiment was done. Figure 11 shows the strains from this load controlled test on the $[(0^{\circ}, 90^{\circ})]_{4s}$ carbon PPS stacking sequence with $\sigma_{\max} = 400\text{ MPa}$, which is about 65% of the tensile strength (Table 2), $\sigma_{\min} = 0$, and a

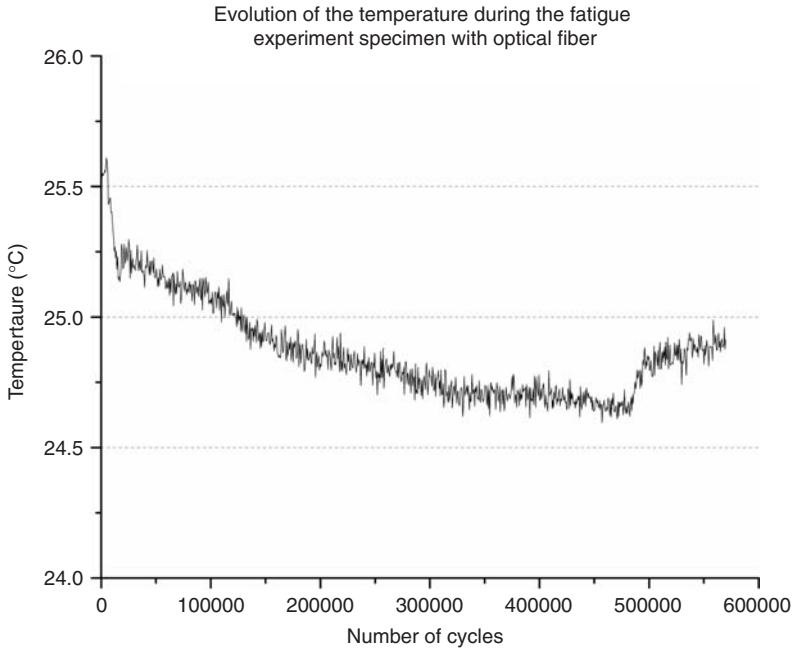


Figure 9. Evolution of the temperature during the fatigue test at 5 Hz for the specimen with optical fiber.

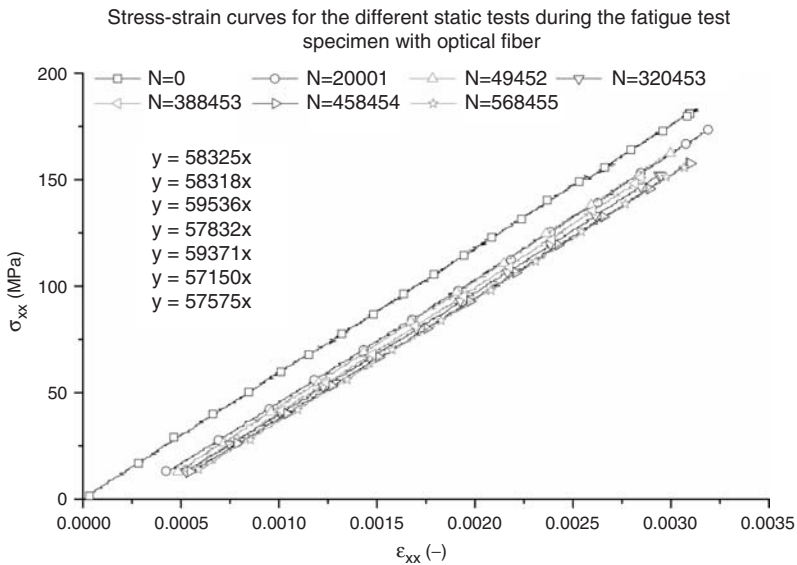


Figure 10. Longitudinal stress as a function of the longitudinal strain for the different static tests; specimen with optical fiber.

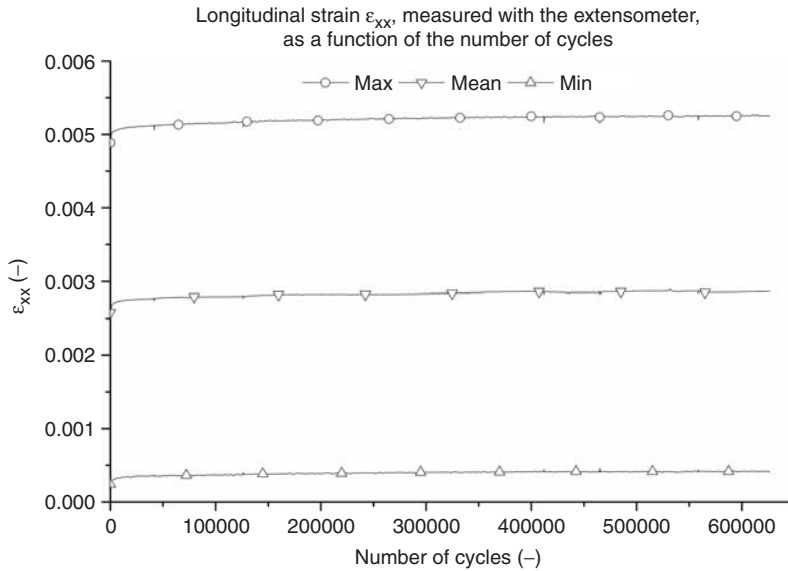


Figure 11. Maximum, minimum and mean value of the strain, measured with the extensometer, during the fatigue experiment.

frequency of 5 Hz. The maximum load was chosen higher than that for the first test, to verify if any permanent degradation or stiffness reduction would occur at this load level. For this specimen, no optical fiber was embedded and the strain was measured using the modified extensometer.

It must be noted that no jumps in the strain occurs, which means that the new design of the blades fulfils its purpose.

During this test, static tests were performed after a certain number of cycles. These stress-strain curves are shown in Figure 12. It can be noted that again, no stiffness reduction or large permanent deformation occurs, even at this higher maximum load level (65% ultimate stress). Therefore, it is safe to assume that at the lower load level also, no degradation occurs. Furthermore, the stiffness is about the same as that for the specimen with the optical fiber. The small deviations are within the normal scatter of the elastic properties of composite materials. Furthermore, other tests have shown no demonstrable difference in fatigue-lifetime or in the ultimate tensile strength in quasi-static tests whether a fiber is embedded or not.

Visualising Damage

In this paragraph, micro-tomography is used to visualize damage in the composite material. Figure 13 shows a 3D-image of carbon fiber-reinforced

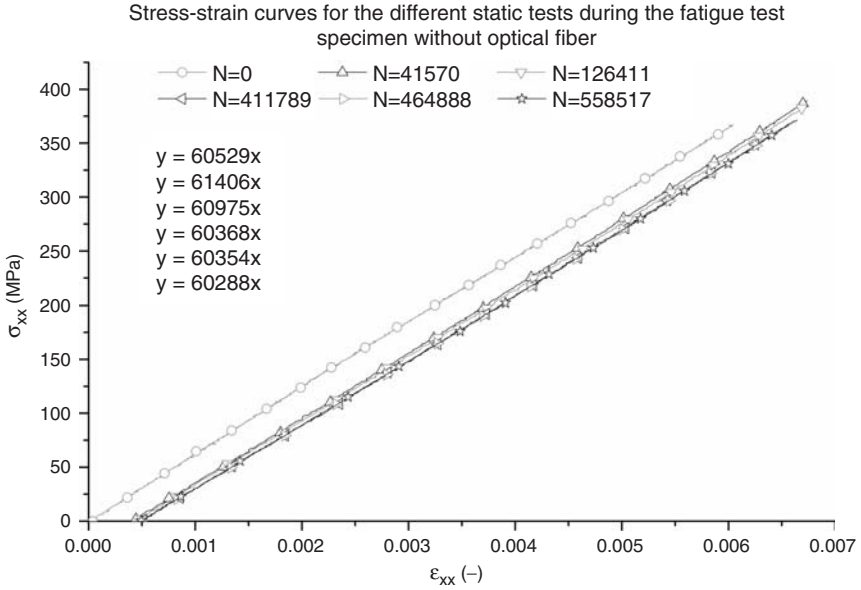


Figure 12. Longitudinal stress as a function of the longitudinal strain for the different static tests. Specimen without optical fiber.

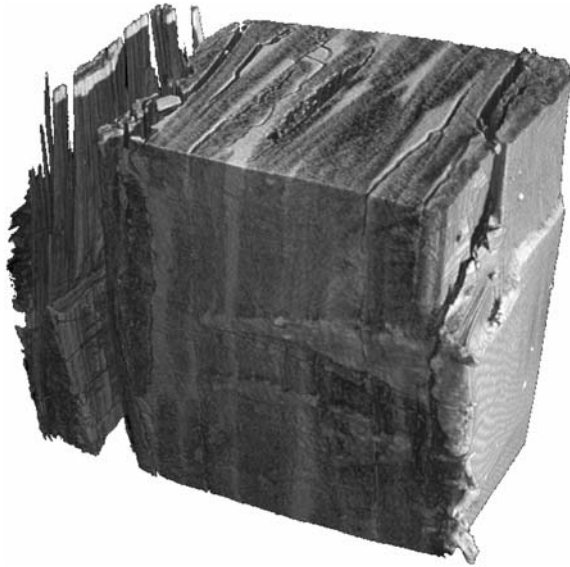


Figure 13. Three-dimensional image of a damaged $[(0^\circ, 90^\circ)]_{4s}$ carbon-PPS.

PPS with $[(0^\circ, 90^\circ)]_{4s}$ stacking sequence that was sawn from a fractured specimen. The different layers of fabric can be distinguished, as well as small matrix cracks and fiber breaking.

CONCLUSIONS

It may be concluded that optical fibers survive over half a million fatigue cycles, which is a lot more than strain gages which tend to de-bond. However, with the SLI 1000 system it is not yet possible to read the optical fiber during fatigue loading with high frequencies. If high sampling rates are required to measure the wavelength during dynamic loading, another setup/device will be necessary which operates at the sample and hold principle.

Since the surface of the used composite is very smooth, a special design of the extensometer blades was presented. These blades have a better grip on the surface of the specimen and therefore, no shifts in the strain measurement occurred during the fatigue loading. The latter was the case with the original blades, making strain-controlled tests unreliable.

Micro-tomography proved to be an interesting tool for the investigation of the micro-structure of composite materials. If the specimen is small enough, the resolution is highly adequate to see the different fiber bundles and the occurring damage.

ACKNOWLEDGMENTS

The authors are highly indebted to the university research fund BOF (Bijzonder Onderzoeksfonds UGent) for sponsoring this research, to Ten Cate Advanced composites for supplying the material and to FOS&S for their material and expertise.

REFERENCES

1. De Waele, V., Degrieck, J., Moerman, W., Taerwe, L. and De Baets, P. (2003). Feasibility of Integrated Optical Fibre Sensors for Condition Monitoring of Composite Structures – Part I: Comparison of Bragg-Sensors and Strain Gauges, *Insight*, **45**(4): 266–271.
2. Degrieck, J., De Waele, W. and Verleysen, P. (2001). Monitoring of Fibre Reinforced Composites with Embedded Optical Fibre Bragg Sensors, With Application to Filament Wound Pressure Vessels, *NDT & E International*, **34**(4): 289–296.
3. Doyle, C., Martin, A., Liu, T., Wu, M., Hayes, S., Crosby, P.A., Powell, G.R., Brooks, D. and Fernando, G.F. (1998). In-situ Process and Condition Monitoring of Advanced Fibre-Reinforced Composite Materials Using Optical Fibre Sensors, *Smart Materials & Structures*, **7**(2): 145–158.

4. Shin, C.S. and Chiang, C.C. (2006). Embedded Fibre Bragg Grating Sensors for Internal Fatigue Damage Monitoring in Polymeric Composites, *Advanced Nondestructive Evaluation I, Pts 1 and 2, Proceedings Key Engineering Materials*, **321–323**: 230–233.
5. Shin, C.S. and Chiang, C.C. (2006). Fatigue Damage Monitoring in Polymeric Composites Using Multiple Fiber Bragg Gratings, *International Journal of Fatigue*, **28**(10): 1315–1321.
6. De Baere, I., Van Paepegem, W., Degrieck, J., Sol, H., Van Hemelrijck, D. and Petreli, A. Comparison of Different Identification Techniques for Measurement of Quasi-Zero Poisson's Ratio of Fabric Reinforced Laminates, *Composites Part A*, **38**(9): 2047–2054.
7. Malo, B., Albert, J., Hill, K.O., Bilodeau, F. and Johnson, D.C. (1994). Effective Index Drift from Molecular Hydrogen Diffusion in Hydrogen-loaded Optical Fibres and its Effect on Bragg Grating Fabrication, *Electronics Letters*, **30**: 442–443.
8. Patrick, H.J., Gilbert, S.L., Lidgard, A. and Gallagher, M.D. (1995). Annealing of Bragg Gratings in Hydrogen-Loaded Optical Fiber, *Journal of Applied Physics*, **78**: 2940–2945.
9. Grattan, K.T.V. and Meggitt, B.T. (2000). *Optical Fibre Sensor Technology: Fundamentals*, Kluwer Academic Publishers, Boston/Dordrecht/London.
10. Chojetzki, C., Rothhardt, M., Müller, H.-R. and Bartelt, H. (2005). *Large Fibre Bragg Grating Arrays for Monitoring Applications – Made by Drawing Tower Inscription*, IPHT, Jena, Germany & FOS&S, Geel, Belgium.
11. Vlassenbroeck, J., Cnudde, V., Dierick, M., Masschaele, B., Van Hoorebeke, L. and Jacobs, P. (2006). Software Tools for Quantification of X-Ray Microtomography at the UGCT, *10th International Symposium on Radiation Physics*, Coimbra, Portugal, 17–22 September 2006.